Vesicle Transport along Microtubular Ribbons and Isolation of Cytoplasmic Dynein from *Paramecium*

Christopher C. Schroeder, Agnes K. Fok, and Richard D. Allen

Pacific Biomedical Research Center and Department of Microbiology, University of Hawaii, Honolulu, Hawaii 96822

Abstract. Cytoplasmic microtubule-based motility in *Paramecium* was investigated using video-enhanced contrast microscopy, the quick-freeze, deep-etch technique, and biochemical isolations. Three distinct vesicle populations were found to be transported unidirectionally along the cytopharyngeal microtubular ribbons. This minus-end–directed movement exhibited unique in vivo features in that the vesicle transport was nonsaltatory, rapid, and predominantly along one side of the microtubular ribbons. To identify candidate motor proteins which may participate in vesicle transport, we prepared cytosolic extracts of *Paramecium* and used bovine brain microtubules as an affinity matrix. These preparations were found to contain a microtubule-stimulated ATPase which supported microtubule gliding in vitro. This protein was verified as a cytoplasmic dynein based upon its relative molecular mass, sedimentation coefficient of 16S, susceptibility to vanadate photocleavage, elevated CTPase/ATPase ratio, and its typical two-headed dynein morphology. This dynein was directly compared with the axonemal dyneins from *Paramecium* and found to differ by five criteria: morphology, sedimentation coefficient, CTPase/ATPase ratio, vanadate cleavage patterns, and polypeptide composition. The cytoplasmic dynein is therefore not an axonemal dynein precursor, but rather it represents a candidate for supporting the microtubule-based vesicle transport which proceeds along the microtubular ribbons.

MICROTUBULE-BASED vesicle transport has been studied in detail in a number of systems including squid axons (Allen et al., 1982, 1985; Brady et al., 1982, 1985; Vale et al., 1985*a–c*), chick embryo fibroblasts (Dabora and Sheetz, 1988), and *Reticulomyxa* (Koonce et al., 1986). The characteristics of vesicle transport along the microtubules were often dependent upon the vesicle size and the cell type being investigated. For example, the larger (0.5–1.0 μm-diam) vesicles in squid axoplasm moved in a saltatory manner and exhibited changes in velocity and direction (Allen et al., 1982). However, the smaller (50-nm-diam) vesicles moved in a smooth and continuous unidirectional manner along the microtubules. Also, using in vitro assays, vesicles have been shown to move smoothly along microtubules in contrast to the saltatory movements visualized in vivo (Vale et al., 1985*c*; Dabora and Sheetz, 1988). The smooth movements observed in vitro were attributed to the lack of an extensively cross-linked cytomatrix which is found in vivo.

The discovery of kinesin (Vale et al., 1985*a*) and cytoplasmic dynein (Paschal et al., 1987) as force-generating microtubule-associated proteins (MAPs)[1] led to the hypothesis that these force-generating enzymes were responsible for vesicle transport along microtubules. Kinesin moves vesicles towards the plus-ends of microtubules (Vale et al., 1985*b*), while cytoplasmic dynein is a minus-end–directed motor (Paschal and Vallee, 1987). The exact role of kinesin and cytoplasmic dynein in vesicle transport has not been unequivocally determined. However, compelling evidence suggests that these two molecules are, at least in part, responsible for vesicle transport along microtubules (Schroer et al., 1988, 1989; Schnapp and Reese, 1989).

The ciliate *Paramecium*, a "primitive" eukaryote, offers an attractive system for the further study of vesicle transport. This organism is easily cultured and can be manipulated readily. Its digestive system membranes have been extensively studied and a clear descriptive picture of vesicle transport along microtubules, and membrane flow and recycling has emerged (Allen, 1984; Fok and Allen, 1988, 1990). Specifically, sequential fusion of digestive system membranes with three vesicular pools (discoidal vesicles, acidosomes, and lysosomes) initiates three separate digestive vacuole stages of the digestive cycle (Allen, 1984). These

Christopher C. Schroeder's present address is the Cell Biology Group, Worcester Foundation for Experimental Biology, Shrewsbury, MA 01545.

This work was presented in preliminary form at the Twenty-ninth Annual Meeting of the American Society for Cell Biology, Houston, TX (Schroeder, C. C., A. K. Fok, and R. D. Allen. 1989. *J. Cell Biol.* 109:82*a* and 109:157*b*).

1. *Abbreviations used in this paper*: MAP, microtubule-associated protein; QF-DE, quick freeze–deep etch.

vesicles are morphologically distinct from one another and monoclonal antibodies have been raised against each vesicular membrane (Fok et al., 1986; Fok and Allen, 1988). This large body of information already obtained for *Paramecium* forms a useful basis for further research on microtubule-based vesicle transport.

An elaborate cytoskeletal architecture near the oral apparatus facilitates the transport of discoidal vesicles towards the cytopharynx where they fuse and provide the membrane for nascent digestive vacuoles (Allen, 1974). This oral cytoskeleton is composed primarily of 40 ribbons of microtubules, each ribbon consisting of 10–12 microtubules lying side by side. The microtubular ribbons arise out of amorphous material associated with a filamentous reticulum at the left edge of the cytopharynx (Allen, 1974). The ribbons are spaced at 1-μm intervals in a perpendicular orientation to the left edge of the cytopharynx, and fan out 20–30 μm into the cytoplasm.

Allen (1974) described the alignment of discoidal vesicles along the microtubular ribbons and reported the firm linkage between the two structures (Allen, 1975), but was unable to visualize their transport because of their small size. In the present study, we used video-enhanced contrast microscopy to visualize the microtubule-based vesicle transport in *Paramecium* and to assay for microtubule-based motility. We report here several unique features of vesicle transport in *Paramecium* which supplement our knowledge of vesicle transport along microtubules. We also describe the isolation and characterization of a cytoplasmic dynein that is distinctly different from the axonemal dyneins isolated from the same organism. We postulate that the cytoplasmic dynein may be an important motor involved with vesicle transport in *Paramecium*.

Materials and Methods

Paramecium multimicronucleatum was cultured in an axenic medium according to Fok and Allen (1979) and harvested at mid-log phase of growth. DEAE-purified tubulin was supplied by Bryce Paschal and Dr. Richard Vallee (Worcester Foundation for Experimental Biology, Shrewsbury, MA). Sea urchin flagellar dynein was provided by Dr. Ian Gibbons (Pacific Biomedical Research Center, Honolulu, HI). Taxol was a gift of Dr. Matthew Suffness (National Cancer Institute, Bethesda, MD). Electrophoresis reagents were obtained from Bio-Rad Laboratories (Richmond, CA). Unless noted, all other reagents were obtained from Sigma Chemical Co. (St. Louis, MO).

Video Microscopy

Free-swimming paramecia were immobilized by gentle compression between a slide and coverslip. Excess fluid was withdrawn with filter paper while microscopically observing the cells. Intracellular vesicle transport was monitored using an Axioplan microscope (Carl Zeiss, Inc.) equipped with differential interference contrast optics. The optical and video train consisted of a 100-W mercury arc lamp, 546-nm interference filter, 1.4 NA condenser, 100×/1.3 NA Plan-neofluar objective, 2× optovar, video camera with Newvicon Tube (model 68; DAGE-MTI, Michigan City, IN), monitor (WV-5410; Panasonic, Secaucus, NJ), 0.5-in. video recorder (model AG6300; Panasonic). Photographs were taken directly from the monitor with a 35-mm camera using a macro lens and Panatomic-X film (Kodak laboratory and Specialty Chemicals, Eastman Kodak Co., Rochester, NY). A 50 lines/in. ronchi ruling (Edmund Scientific Co., Barrington, NJ) was used in front of the camera lens to filter out the video scan lines.

Quick freeze–Deep etch (QF-DE) Electron Microscopy

Living paramecia were quick-frozen, fractured, and etched as previously described (Allen et al., 1989). Briefly, living paramecia were pelleted using a clinical centrifuge at full speed for 1 min. The cell pellet was impact frozen against a highly polished copper block cooled by liquid nitrogen to −195°C using a rapid freezing device (model KF-80; Reichert Jung, Vienna, Austria) equipped with an MM80 pneumatic head. The frozen sample was fractured within 20 μm of the frozen surface and etched at −95°C for 4–6 min in a freeze-etch apparatus (model 401; Balzers, Hudson, NH). A replica was made by shadowing platinum from an angle of 24° and carbon from 80° onto the rotating specimen. The replica was removed and cleaned through a succession of bleach, chromic acid, and finally distilled water. The replicas were picked up on Formvar-coated slot grids and examined at 80 kV in an electron microscope (model 10A; Carl Zeiss, Inc.). Micrographs were printed in reverse contrast so that raised areas appear white against a black background.

Preparation of MAP-free Bovine Brain Microtubules

The taxol isolation procedure of Vallee (1982, 1986) was used to isolate microtubules. The purified microtubules were washed once with PEM buffer (0.1 M Pipes, 1 mM $MgSO_4$, 1 mM EGTA, pH 6.6) and twice with PEM containing 10 mM MgATP and 0.36 M NaCl to release any bound MAPs or motor proteins. The resultant pellet was virtually pure tubulin, free of contaminating proteins. The microtubules were frozen in liquid nitrogen and stored at −80°C until use.

Cytoplasmic Dynein Isolation

5 or 10 liters of cells were harvested using a cream separator and concentrated to a pellet using a clinical centrifuge. After washing twice with cold PEM buffer the cell pellet was resuspended in an equal volume of PEM buffer containing 0.1 mg/ml soybean trypsin inhibitor, 2 mM PMSF, and 1 mM DTT. Unless otherwise noted, all subsequent manipulations were performed at 4°C. Cells were homogenized to ~80% breakage using a ball-bearing homogenizer (Berni-tech Engineering, Saratoga, CA). The homogenate was centrifuged at 40,000 *g* for 30 min at 4°C. The supernatant was recovered and centrifuged at 150,000 *g* for 1 h at 4°C. The supernatant, or cytosolic extract, was recovered and the volume measured. Hexokinase (36 U/ml) and glucose (9 mM) were added and the mixture was incubated for 15 min at room temperature to deplete endogenous ATP. MAP-free bovine brain microtubules and taxol were added at concentrations of 0.3 mg/ml and 20 μM, respectively, and the mixture was incubated on ice for 25 min to allow the dynein to bind to the microtubules. An additional 5-min incubation at 37°C was included to insure the complete polymerization of the microtubules. The microtubule/dynein pellet obtained by centrifugation at 40,000 *g* for 30 min at 4°C was resuspended with PEM buffer and recentrifuged. The washed pellet was resuspended to one fifth of the volume of the original cytosolic extract with PEM containing 10 μM taxol. The dynein was released from the microtubules by the addition of 10 mM MgATP. After a 20-min incubation at room temperature, the microtubules were pelleted as above. Cytoplasmic dynein was recovered in the supernate and concentrated in a microconcentrator (Centricon 30; Amicon Corp., Danvers, MA). The concentrated ATP-sensitive extract was layered on a 5-ml linear sucrose gradient (5–20%) in sodium acetate buffer (10 mM Tris, pH 7.2, 100 mM sodium acetate, 3 mM magnesium sulfate, 1 mM EGTA, 1 mM DTT) and centrifuged for 14 h at 75,000 *g* at 4°C in a rotor (model SW 50.1; Beckman Instruments, Inc., Palo Alto, CA). The gradient was fractionated from the bottom, and 0.4-ml fractions were collected.

Axonemal Dynein Isolation

Cells were harvested and pelleted as described above for the isolation of cytoplasmic dynein. Cilia were isolated according to Adoutte et al. (1980) and the dynein was extracted as described by Bell et al. (1982) with minor modifications. The cells were first washed with cold Dryl's solution (1 mM Na_2HPO_4, 1 mM NaH_2PO_4, 2 mM $Na_3C_6H_5O_7$, 1.5 mM $CaCl_2$, pH 6.5) to induce trichocyst firing, and the cell pellet was resuspended in 5 pellet volumes of Dryl's solution. An equal volume of STEN (0.5 M sucrose, 20 mM Tris, pH 7.5, 2 mM EDTA, 6 mM NaCl) was added and incubated for 10 min on ice. Deciliation was initiated with the addition of 10 mM $CaCl_2$ and 30 mM KCl, and continued for an additional 15 min. The cell bodies were pelleted at half speed in a clinical centrifuge and the supernate containing cilia was recovered and centrifuged at 27,000 *g* for 20 min at 4°C. The cilia were washed twice in sodium acetate buffer, and then resuspended to the original cell pellet volume. The cilia were demembranated by incubation in 1% Triton X-100 in sodium acetate buffer for 30 min on ice. The axonemes were washed twice with buffer to remove the membrane fraction.

The resultant pellet was resuspended to one half of the original cell pellet volume with high salt extraction buffer (0.6 M NaCl in sodium acetate buffer) and incubated for 15 min on ice to release the dynein. The axonemes were pelleted at 40,000 *g* for 30 min at 4°C and the dynein was recovered in the supernatant and concentrated in a Centricon 30 microconcentrator. The concentrated dynein extract was layered on a linear sucrose gradient (5–25%) in sodium acetate buffer and centrifuged for 12 h at 75,000 *g* at 4°C and fractionated.

Vanadate Photocleavage

The procedure of Gibbons et al. (1987) was used. Briefly, vanadate and MgATP, both at 150 μM final concentration, were added to the sucrose gradient-purified dyneins. Controls contained MgATP but no vanadate. The samples and controls were irradiated for 1 h on ice with a 365-nm UV light from a distance of ~5 cm.

In Vitro Motility Assay

The assay of Vale and Toyoshima (1989) using a flow chamber was used. Two successive aliquots of sucrose gradient purified cytoplasmic dynein were allowed to adsorb for 2 min each. The flow chamber was washed with 75 μl of motility buffer (40 mM KCl, 1 mM EGTA, 3 mM $MgCl_2$, 10 mM Tris, pH 7.4). A solution of 0.02 mg/ml DEAE-purified, taxol-stabilized microtubules and 1 mM ATP in motility buffer was introduced into the chamber and observed with a Universal microscope (Carl Zeiss, Inc.). The optical and video train was similar to the Axioplan described above except for a 100×/1.25 NA Planachromat objective and a video camera (model 67 m; Dage-MTI). Continuous background subtraction and contrast enhancement was performed using an image analysis system (Image 1/AT; Universal Imaging, Media, PA).

Ultrastructural Analysis of Isolated Proteins

Negative staining was performed as described by Marchese-Ragona et al. (1988). A carbon film was evaporated onto freshly cleaved mica. The carbon film was floated onto sucrose gradient-purified dynein samples diluted to 10–20 μg/ml with sodium acetate buffer. The film was transferred to a drop of aqueous uranyl acetate (1%) and picked up on uncoated mesh grids (Ted Pella, Inc., Redding, CA). The grids were then allowed to air dry and viewed in an electron microscope (Model 10A; Carl Zeiss, Inc.) operated at 80 kV.

Other Biochemical Procedures

Protein determination was performed using the Bio-Rad protein assay. SDS-PAGE was performed according to Laemmli (1970) under denaturing and reducing conditions and the gels were stained with either Coomassie brilliant blue R-250 or the silver staining procedure of Merril et al. (1981). The malachite green method for the detection of inorganic phosphate (Lanzetta et al., 1979) was used for the ATPase and CTPase assays. Sedimentation coefficients were determined as described by Martin and Ames (1961).

Results

Vesicle Transport along the Microtubular Ribbons

Video-enhanced contrast microscopy of immobilized *Paramecium* allowed the direct observation of vesicle transport along the cytopharyngeal microtubular ribbons. When the cells were positioned on their left or ventral side, the microtubular ribbons radiated out perpendicular to the cytopharynx so that only the edges of the microtubular ribbons were visible.

Two groups of vesicles were selectively transported along the microtubular ribbons (Fig. 1). The first group of vesicles was small and flattened with dimensions of 0.1 × 0.6 μm. These flat vesicles were barely discernible and appeared as moving bumps on the surface of the microtubular ribbon. The second group of vesicles was spherical with diameters ranging from 0.5 to 1.2 μm. These large vesicles were prominent and served as the general indicator for vesicle transport. Other recognizable organelles such as mitochondria and trichocysts were visible in this area, but they were not transported along the microtubular ribbons. The best observations of vesicle transport were made immediately after compression of the cells. Vesicle transport along the microtubular ribbons was only visible for a distance of ~10 μm extending from the cytopharynx. Vesicle movement was primarily unidirectional towards the cytopharynx and was smooth, continuous, and seemingly fed by a never-ending source of vesicles. Occasionally, vesicles moved away from the cytopharynx, but this movement was rare. All vesicles travelled at approximately the same rate, which was determined to be 5.8 ± 0.9 μm/s. In no instance did a vesicle "pass" another or stop and reverse directions.

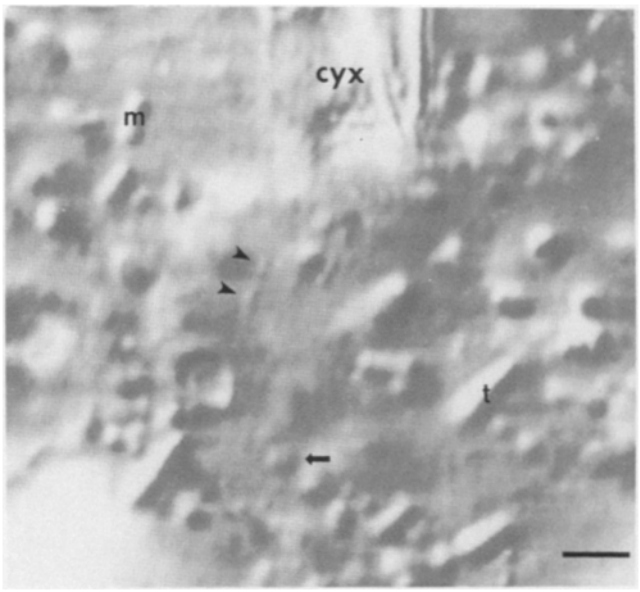

Figure 1. Video micrograph of vesicles selectively transported along the microtubular ribbons. Small flattened vesicles (*arrowheads*) and large spherical vesicles (*arrow*) were found to move smoothly and rapidly (5.8 μm/s) toward the cytopharynx (*cyx*) or oral region. The microtubular ribbons are barely visible at this magnification. Other recognizable organelles including mitochondria (*m*) and trichocysts (*t*) were present in this general area, but were not transported along the microtubular ribbons. Bar, 2.5 μm.

An interesting pattern of transport was observed when both the moving vesicles and the adjacent microtubular ribbon were visible (Fig. 2). Vesicles moving toward the cytopharynx appeared to travel along the anterior side of the microtubular ribbon. In contrast, vesicle movement away from the cytopharynx appeared to occur along the posterior side of the microtubular ribbon. A schematic diagram of vesicle transport along the microtubular ribbons is presented in Fig. 3.

We attempted to specifically inhibit this vesicle transport by exposure to vanadate after gentle permeabilization. However, the cells were very sensitive to perturbation and an appropriate buffer system to study vesicle transport inhibition and reactivation was not found. Therefore, discriminating between the nonspecific effects of the permeabilizing buffer and the inhibitory reagent used was not possible.

To obtain a faithful representation at the ultrastructural

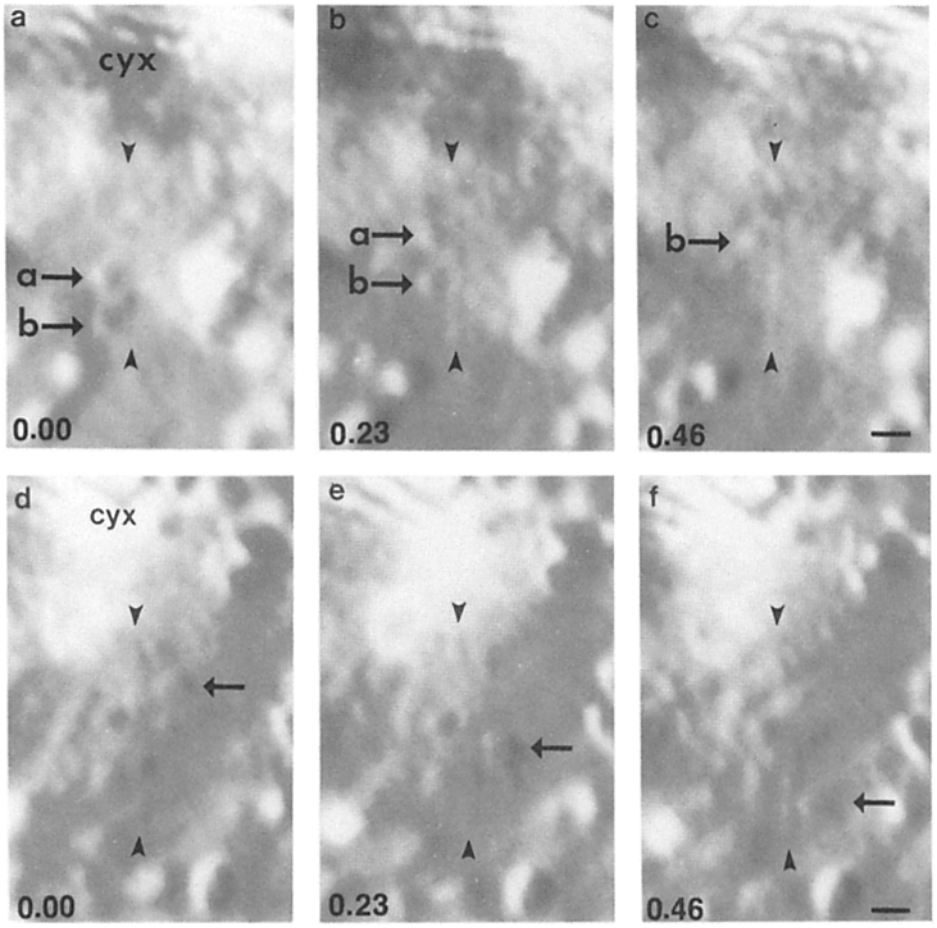

Figure 2. Vesicle transport along the microtubular ribbons. Three successive video frames (*a–c*) illustrate two vesicles (*a* and *b*) as they move toward the cytopharynx (*cyx*) along a microtubular ribbon (between *arrowheads*). Note that both vesicles are on the same side of the microtubular ribbon which was determined to be the anterior side. The second set of three video frames (*d–f*) illustrates a vesicle (*arrow*) moving away from the cytopharynx. Note that the vesicle is on the posterior side of the microtubular ribbon. Time between frames in seconds is indicated. Bar, 1 μm.

level of the components involved in vesicle transport along the microtubular ribbons, the QF-DE technique was used. This technique enabled the observation of cellular ultrastructure in its near-native condition. The granular appearance of the cytoplasm indicated that the cells were well preserved, particularly in shallow fractures through the cell cortex. Although slightly deeper fractures were required to expose the oral region, the structural preservation was still adequate.

Fractures through the oral region revealed structures such as the microtubular ribbons, the cytopharynx membrane, and discoidal vesicles (Fig. 4). Each microtubular ribbon was composed of several microtubules lying side by side forming a planar ribbon (Fig. 4, *inset*). Adjacent microtubules in the ribbon were extensively linked by fine cross-bridges. Using the hook decoration procedure (Heidemann and McIntosh, 1980), the minus-ends of these microtubules were determined to be at the cytopharynx (data not shown). Thus, vesicle transport along the microtubular ribbons was primarily minus-end directed, although occasional plus-end directed movements were seen.

The discoidal vesicles were indeed flattened vesicles as previously described. Their E-fracture face was identical in its particulate appearance to that of the E-fracture face of the cytopharynx membrane. The discoidal vesicles were aligned single file along the microtubular ribbons (Fig. 4). As with video microscopy, they were almost exclusively located on the anterior side of the ribbons maintaining a constant spacing of 30–40 nm from the microtubular ribbon. At high magnifications, cross-bridges were evident between the discoidal vesicles and the ribbons (Fig. 4, *arrow*).

The acidosome morphology after the QF-DE technique was quite distinct from other vesicles making them easily recognizable. Their smooth E-fracture face and particulate P-fracture face has been described previously (Allen and Fok, 1983*a*). However, the QF-DE technique illustrated a unique luminal etching pattern for the acidosome, thus providing an additional marker for the identification of acidosomes throughout the cytoplasm (Fig. 5 *a*). The acidosomes, which varied in size from 0.15 to 1 μm in diameter, were also found along the anterior sides of the microtubular ribbons.

A third population of previously unidentified small vesicles was detected using the QF-DE technique (Fig. 5, *b* and *c*). These vesicles measured 100 nm in diameter and were found to be intermixed with discoidal vesicles and acidosomes on the anterior side of the microtubular ribbons. The E-fracture face of these 100-nm vesicles was smooth and nearly identical in appearance to the acidosome E-fracture face. Because of their small size they were rarely found in cross fracture so their lumens were not characterized. These vesicles also maintained a constant 30–40-nm spacing from the microtubular ribbons and intervening cross-bridges were very prominent (Fig. 5, *b*, *arrows*).

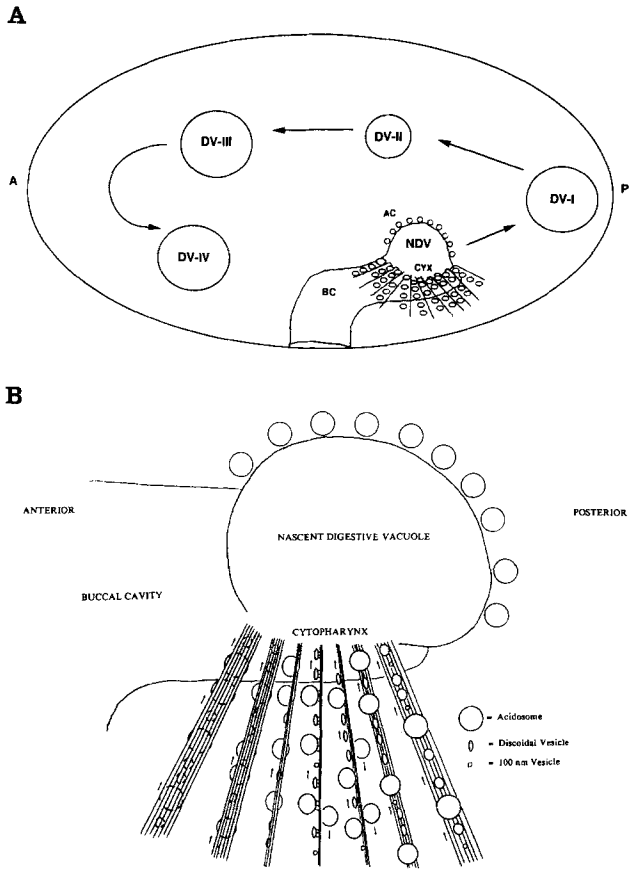

Figure 3. Schematic diagrams of vesicle transport along the microtubular ribbons. *A* illustrates the site of formation and general movements of digestive vacuoles (*DV-I* to *DV-IV*) in *Paramecium*. *B* illustrates the movement of vesicles (acidosomes, discoidal vesicles, and 100-nm vesicles) along the anterior side of the microtubular ribbons.

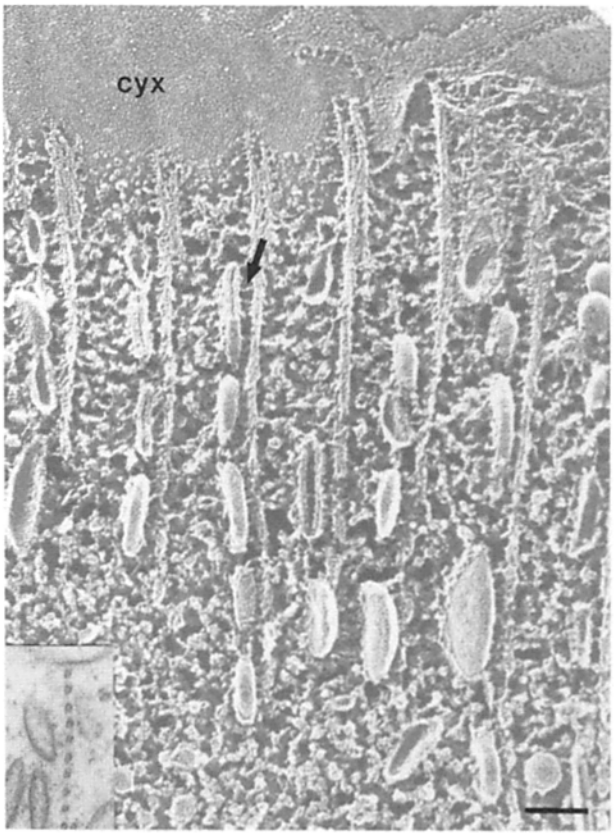

Figure 4. QF-DE fracture through the oral region. The edges of several microtubular ribbons extend away from the cytopharynx membrane (*cyx*). The discoidal vesicles are closely aligned with the anterior side of the microtubular ribbons. Cross-bridges are evident between the vesicles and microtubules (*arrow*). Bar, 0.2 μm. (*Inset*) Cross section of a single microtubular ribbon to illustrate the planar nature of the ribbon. Discoidal vesicles are present on the anterior side of the ribbon. Same magnification as Fig. 4. (Thin-sectioned material was prepared as described by Allen, 1974).

Cytoplasmic Dynein Isolation

The existence of microtubule-based vesicle transport suggested the presence of a microtubule-based motor in *Paramecium*. A purification scheme modified from published procedures (Paschal et al., 1987; Schnapp and Reese, 1989; Euteneuer et al., 1988), was used to isolate putative microtubule-based motors present in the cytosol of *Paramecium*. By using microtubule affinity purification, a high molecular mass (>350 kD), nucleotide-sensitive binding protein was isolated from a high speed cytosolic extract (Fig. 6). The isolation of this protein was strictly dependent upon the depletion of endogenous ATP from the cytosolic extract and the addition of exogenous microtubules. The protein was further purified by sucrose density gradient centrifugation which separated it from tubulin and other contaminants present in the ATP extract.

On SDS-PAGE the high molecular mass protein had the same relative mobility as sea urchin flagellar dynein and bovine brain cytoplasmic dynein. Vanadate photocleavage produced two cleavage fragments of ~165 kD and 200 kD, verifying the protein as a dynein-like molecule (Fig. 7, lanes *3* and *4*). Comparison with thyroglobulin centrifuged in 5–20% sucrose gradients indicated a sedimentation coefficient of ~16S for the cytoplasmic dynein.

The ATPase and CTPase activities of the sucrose gradient–purified protein were determined (Table I). Both the ATP extract and sucrose gradient–purified samples were tested in their ability to couple ATP hydrolysis to force generation using an in vitro motility assay. Both the ATP extract and the sucrose gradient fractions promoted the binding of microtubules to the coverslip. The peak gradient fractions also supported microtubule gliding at a rate of 2.72 ± 0.18 μm/s (Fig. 8).

Visualization of the isolated protein by negative stain or low angle rotary shadowing revealed a two headed "v"-shaped molecule (Fig. 9). The globular heads measured 15.2 ± 1.6 nm and were connected to an amorphous base by thin stems. Occasionally, thin projections emanating from the globular heads were evident. The overall width and height of the negatively stained molecules ranged from 28 to 57 nm wide by 35 to 40 nm high. The prominence of the base and stems varied considerably.

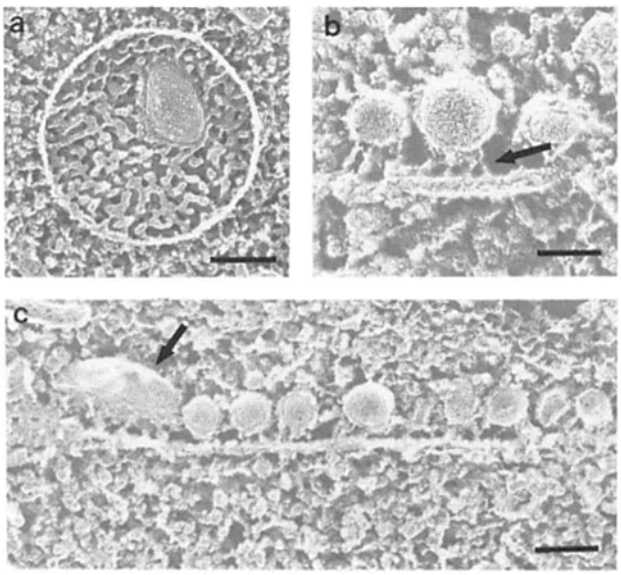

Figure 5. Other vesicles transported along the microtubular ribbons. *a* illustrates the unique luminal etching pattern for the acidosome. *b* illustrates the 100-nm vesicle and the regular cross-bridges (*arrow*) between the vesicle and the microtubular ribbon. *c* illustrates the 100-nm vesicles aligned along the microtubular ribbon. A discoidal vesicle (*arrow*) is also present. Again note that the vesicles are only on one side. Bars: (*a* and *c*) 0.25 μm; (*b*) 100 nm.

Comparison to Axonemal Dyneins

Because paramecia are ciliated cells and have ciliary dyneins, the *Paramecium* cytoplasmic and axonemal dyneins were compared by several different criteria to ensure the cytoplasmic dynein was not an axonemal precursor. Salt extraction of *Paramecium* axonemes and purification on sucrose gradients yielded two dynein species. The two dyneins corresponded to the 22S and 12S species identified in *P. tetraurelia* (Travis and Nelson, 1988). Negative stain EM revealed a three-headed molecule for the 22S dynein and a single-headed molecule for the 12S dynein (Fig. 10). The ATPase and CTPase activities of the two axonemal dynein species are shown in Table I. Although the CTPase was higher than reported for *Tetrahymena* axonemal dyneins (Shimizu, 1987), the *Paramecium* axonemal dyneins did not show an elevated CTPase/ATPase ratio. In addition, the vanadate cleavage patterns (Fig. 7) and polypeptide composition of the axonemal dyneins were different from the cytoplasmic dynein.

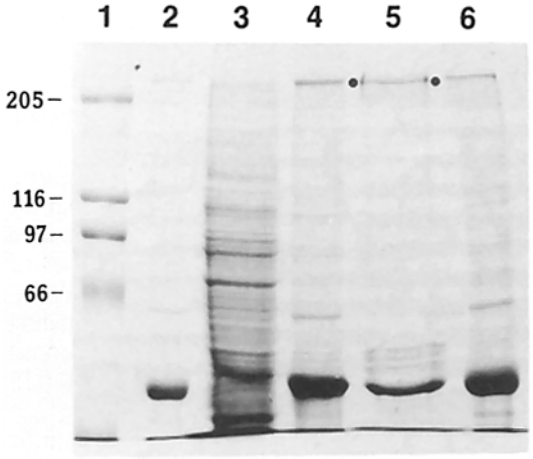

Figure 6. Purification of cytoplasmic dynein. MAP-free, bovine brain microtubules (lane *2*) were mixed with an ATP-depleted, high-speed cytosolic extract from *Paramecium* (lane *3*). The pelleted and resuspended microtubules (lane *4*) were extracted with MgATP and centrifuged to yield a supernatant (lane *5*) and pellet (lane *6*). The ATP extract (lane *5*) contained cytoplasmic dynein (•) and a varying amount of tubulin and other contaminating polypeptides. Molecular weight standards (lane *1*) are indicated by their relative molecular weights ($\times 10^3$).

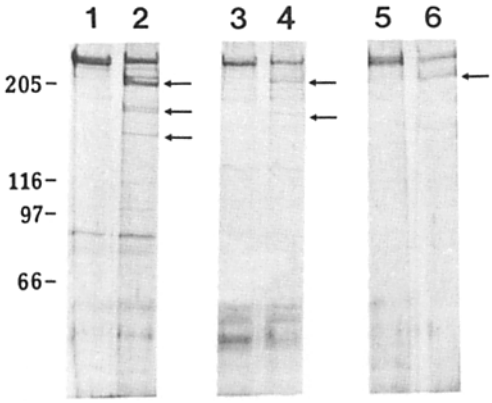

Figure 7. Vanadate cleavage patterns of *Paramecium* cytoplasmic and axonemal dyneins. Peak sucrose gradient fractions of 22S axonemal dynein (lanes *1* and *2*), cytoplasmic dynein (lanes *3* and *4*), and 12S axonemal dynein (lanes *5* and *6*) were subjected to vanadate photocleavage. Lanes *1*, *3*, and *5* represent the control lanes, while lanes 2, *4*, and *6* were the cleavage lanes. Note the strikingly different cleavage fragments produced (*arrows*) for the three dynein species. Some proteolysis of the cytoplasmic dynein occurred which gave rise to the additional high molecular weight bands in lanes *3* and *4*.

Discussion

Characterization of Vesicle Transport

Two distinct vesicle populations were observed by video microscopy to move along the microtubular ribbons that are joined to the cytopharynx in *Paramecium*. The small flattened vesicles correspond to discoidal vesicles based on their morphology and location along the microtubular ribbons (Allen, 1974, 1975). The larger spherical vesicles are identified as acidosomes by their size and EM morphology (Allen and Fok, 1983, *a*, *b*). This is the first indication that acidosomes are translocated in a microtubule-dependent manner. A different function for each of these vesicle populations in *Paramecium* has been established (Allen, 1974; Allen and Fok, 1983, *a*, *b*), and their transport in the manner described is compatible with these functional roles.

Because the discoidal vesicles and acidosomes are selectively transported along the microtubular ribbons while other vesicle populations are not, a specific recognition between these vesicles and the microtubular ribbons is suggested. The nature of this recognition is unknown, but seems

*Table I. ATPase and CTPase Activities of Cytoplasmic and Axonemal Dyneins**

	ATPase	CTPase	CTPase/ATPase
Cytoplasmic dynein‡	347 ± 80 (8)§	474 ± 24 (2)	1.4
22S axonemal dynein	286 ± 96 (4)	206 ± 58 (2)	0.7
12S axonemal dynein	250 ± 42 (2)	163 ± 42 (2)	0.7

* Specific activities were presented as nmol/min per mg protein.
‡ The specific activity of cytoplasmic dynein was stimulated an additional ~4.0-fold by taxol-stabilized microtubules at a final concentration of 0.2 mg/ml and inhibited 57% by 20 μM vanadate.
§ Parentheses refer to number of experiments.

unique because, in other systems, a multitude of vesicle types have been reported to be transported along a single microtubule (Allen et al., 1982; Brady et al., 1982; Vale et al., 1985*c*). The well-defined vesicles of *Paramecium* offer a unique opportunity to investigate microtubule–vesicle recognition and transport.

The QF-DE analysis identified a third population of 100-nm vesicles bound to the microtubular ribbons. These vesicles are most likely too small to be recognized in living *Paramecium* using our video microscope system. The function of these 100-nm vesicles is unknown. The morphology of their E-fracture face and their association with the microtubular ribbons suggest the 100-nm vesicles may be acidosome precursor vesicles which coalesce to form the large acidosomes. As the origin of the acidosome remains unknown, it is tempting to view these 100-nm vesicles as acidosome precursors.

The characteristics of the vesicle transport along the microtubular ribbons were unexpected. The rate of vesicle transport along the microtubular ribbons (5.8 μm/s) is faster than axonal transport visualized directly either in vivo (2.5 μm/s; Allen et al., 1982) or in vitro (2.2 μm/s, Vale et al., 1985*c*) and considerably faster than the speed of transport in tissue culture cells (0.4 μm/s; Dabora and Sheetz, 1988). Only *Reticulomyxa*, a freshwater ameba, has similar or higher rates of vesicle transport (up to 20 μm/s; Koonce et al., 1986).

The smooth nature of transport along the microtubular ribbons is also in contrast to most in vivo systems. Vesicle transport in living cells or tissue is classically described as saltatory or exhibiting frequent stops, starts, reversals in direction, and changes in velocity (Rebhun, 1972; Dabora and Sheetz, 1988). This is especially true for the larger transported vesicles. Only in the extruded axons and other in vitro systems has the transport of large vesicles been described as smooth and continuous (Vale et al., 1985*c*; Dabora and Sheetz, 1988).

The most interesting phenomenon of vesicle transport along the microtubular ribbons in paramecia is the sidedness with respect to the direction of transport. This observation was initially suggested by Allen (1974). To reiterate, vesicles

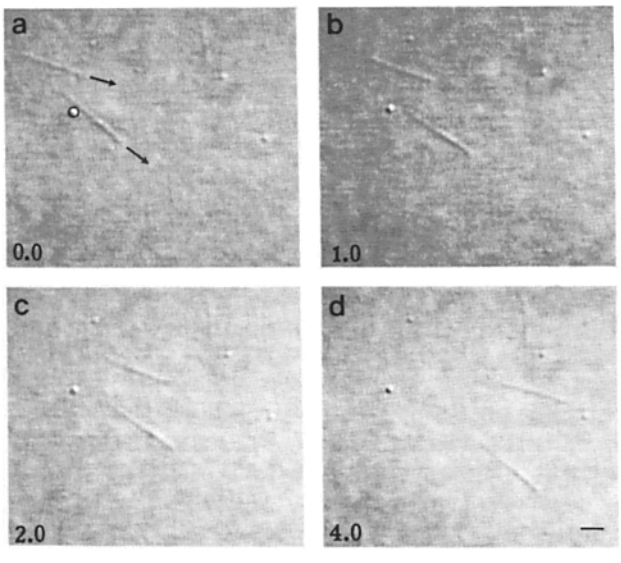

Figure 8. Microtubule gliding induced by cytoplasmic dynein. Two microtubules are gliding at ~2.7 μm/s across a dynein-coated coverslip. A stationary particle (*circled*) may be used as a reference point. The time between frames in seconds is indicated. Bar, 2 μm.

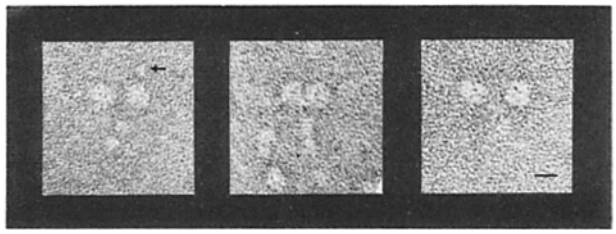

Figure 9. Negatively stained images of cytoplasmic dynein from *Paramecium*. Two ~15-nm globular heads are connected by thin stems to an amorphous base. Occasionally, small projections (*arrow* in left panel) protrude from the globular heads. Bar, 15 nm.

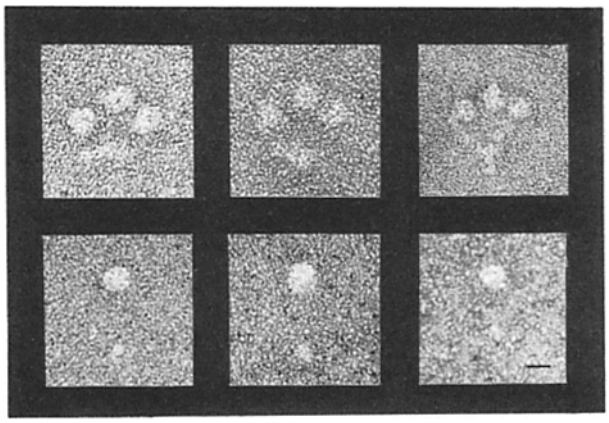

Figure 10. Negatively stained images of *Paramecium* axonemal dyneins. The 22S axonemal dynein (*top row*) is a three-headed dynein while the 12S axonemal dynein (*bottom row*) is a single-headed dynein. Bar, 15 nm.

(both discoidal vesicles and acidosomes) moving toward the cytopharynx appear to do so along the anterior side of the microtubular ribbons. Vesicles that occasionally move away from the cytopharynx do so along the posterior side of the microtubular ribbons. This observation is supported at the ultrastructural level using the QF-DE technique which halts cellular processes instantaneously. Discoidal vesicles, acidosomes, and 100-nm vesicles are all found to be located almost exclusively on the anterior side of the microtubular ribbons. Unidirectional movement toward the cytopharynx along the anterior side would favor their transport to the cytopharynx.

The three characteristics of transport (rate, smooth nature, and sidedness) can be partially explained by the elaborate nature of the microtubular ribbons. Because the microtubular ribbons are planar sheets of cross-linked microtubules lying side by side, a particular vesicle does not have access to 360° of the microtubule as it might with a single microtubule. Thus, vesicle transport along these ribbons is restricted to either one side of the ribbon or the other, which partially explains the sidedness of transport. Similarly, there may be long, fibrous MAPs (such as MAP-2) present along the posterior side of the microtubular ribbons which, in other systems, have been shown to interfere with the binding of microtubule-based motors to microtubules (Paschal et al., 1989). The presence of such MAPs could alter transport along the posterior side of the ribbon. The mechanism for such an asymmetric arrangement of MAPs along a microtubule is not without precedent. Axonemal dynein is linearly arranged along the A subfiber of the axoneme indicating that such an arrangement is possible.

The smooth nature and rapid rate of vesicle transport may be influenced by the contact of each vesicle with the microtubular ribbons. Because the microtubular ribbon is a sheet of microtubules, each vesicle can be in potential contact with up to 12 microtubules rather than a single microtubule, as is common for other systems. Therefore, there may be a larger number of motor molecules propelling each discoidal vesicle and acidosome in *Paramecium*. The more motors that are involved, the greater the chance that more than one motor connects the vesicle to the microtubular ribbon at all times which could give rise to a smoother and more rapid rate of transport of vesicles. Vale and Toyoshima (1989) showed that rate of microtubule gliding increases by increasing the concentration of dynein molecules adsorbed to the glass coverslip in an in vitro assay. Thus, it might be expected that below the number of contacts needed to give a maximum rate of transport, the more dynein molecules involved with translocation, the higher the transport rate.

Characterization of Cytoplasmic Dynein

With the multitude of microtubule-based movements in *Paramecium*, we attempted to isolate a microtubule-based motor powering such movements. By exploiting the affinity of known microtubule-based motors for microtubules in the absence of ATP, an isolation scheme was developed to isolate such a motor from the cytosol of *Paramecium*. Using this method we were able to purify and characterize a cytoplasmic dynein. The physical, structural, and enzymatic properties of this molecule are similar to those of the cytoplasmic dyneins isolated from brain tissue (Paschal et al., 1987; Shpetner et al., 1988; Vallee et al., 1988), squid axons (Schnapp and Reese, 1989), testis (Neely and Boekelheide, 1988; Neely et al., 1990) liver (Collins and Vallee, 1990), *Dictyostelium* (Koonce and McIntosh, 1989), and a dynein-like molecule from *Reticulomyxa* (Euteneuer et al., 1988).

The properties of this molecule—heavy chains of >350 kD, an ATPase activity that is sensitive to low concentrations of vanadate, and the vanadate-mediated photocleavage of its heavy chains—are all classical dynein-like properties (Gibbons, 1989). The structural characterization, which reveals a two-headed dynein morphology, also supports a dynein classification for this molecule. This two-headed structure is identical to the cytoplasmic dyneins of neuronal tissue (Vallee et al., 1988; Schnapp and Reese, 1989) and rat testis (Neely et al., 1990).

Another characteristic property of cytoplasmic dyneins is their ability to hydrolyze the nucleotide CTP at a higher rate than the hydrolysis of ATP (Shpetner et al., 1988; Collins and Vallee, 1989; Koonce and McIntosh, 1990). Although the CTPase/ATPase ratio is not as high as with brain cytoplasmic dynein, the cytoplasmic dynein from *Paramecium* fulfills this criterion. In addition, this cytoplasmic dynein is capable of ATP-coupled force production as demonstrated using an in vitro motility assay.

However, because paramecia have cilia, it was necessary to demonstrate that the cytoplasmic dynein was not a ciliary precursor. By five separate criteria (morphology, sedimentation coefficient, CTPase/ATPase ratio, vanadate cleavage patterns, and polypeptide composition) the cytoplasmic dynein shows significant differences from the two axonemal dynein species. Therefore it is reasonable to conclude that the cytoplasmic dynein is not a ciliary precursor, but rather a distinct dynein species and may therefore participate in cytoplasmic microtubule-based motility.

Several other laboratories have previously compared different isoforms of dynein from unfertilized sea urchin eggs to distinguish between ciliary/flagellar precursors and cytoplasmic isoforms of dynein (Pratt, 1986; Porter et al., 1988; Foltz and Asai, 1988). Our findings clearly support the hypothesis that one isoform of dynein participates in ciliary motility, while another isoform of dynein exists and may function exclusively as a cytoplasmic enzyme.

It is becoming clear that cytoplasmic dyneins play a major role in the microtubule-based transport of vesicular organelles. Vanadate photocleavage of cytosolic extracts from either cultured cells (Schroer et al., 1989) or squid axons (Schnapp and Reese, 1989) inhibits minus-end-directed vesicle transport along microtubules. The addition of chick brain cytoplasmic dynein is able to restore the minus-end-directed transport in the cultured cell extracts. Also, cytoplasmic dynein has been localized on the surface of membranous organelles in the axon (Hirokawa et al., 1990). The *Paramecium* cytoplasmic dynein may perform a similar vesicle transport function such as the transport of the discoidal vesicles and acidosomes along the microtubular ribbons.

Cytoplasmic dyneins are minus-end-directed motors (Paschal and Vallee, 1987). The minus-ends of the microtubular ribbons in *Paramecium* are at the cytopharynx; thus much of the transport along the microtubular ribbons is minus-end directed and could be mediated by cytoplasmic dy-

nein. The rapid rate of vesicle transport also favors a dynein-like motor as opposed to a kinesin-like motor. However, the bidirectional transport along the microtubular ribbons would require either two distinct motors or a bidirectional motor as found in *Reticulomyxa* (Euteneuer et al., 1988).

In summary, we have examined the microtubule-based vesicle transport in *Paramecium* using video microscopy and the QF-DE technique. We have also isolated a cytoplasmic dynein which is a strong candidate for being a vesicle motor, as suggested in other systems. This study also demonstrates that microtubule-based vesicle transport in a "primitive" eukaryote such as *Paramecium* is probably not unlike microtubule-based vesicle transport in higher organisms. In addition, there are a number of distinguishing features of this system which make it another useful model system for studying microtubule-based vesicle transport. The data also expand our knowledge of the events leading to digestive vacuole formation in *Paramecium* and support the role of microtubule-based motility in membrane recycling of this organism.

We would like to thank Dr. Bill Saxton (Department of Biology, Indiana University, Bloomington, IN) for assistance with the video microscopy. We are also grateful to Dr. Ian Gibbons and Dr. Grace Tang (Pacific Biomedical Research Center, Honolulu, HI) for many helpful discussions, and Bryce Paschal for critical reading of the manuscript.

This work was supported by National Science Foundation grants DCB 87-18598 and DCB 88-19182, and National Institutes of Health Minority Access to Research Careers grant GM 07684, and Research Careers in Minority Institutes grant RR 03061.

Received for publication 29 May 1990 and in revised form 9 July 1990.

References

Adoutte, A., R. Ramanathan, R. M. Lewis, R. R. Dute, K.-Y. Ling, C. Kung, and D. L. Nelson. 1980. Biochemical studies of the excitable membrane of *Paramecium tetraurelia*. III. Proteins of cilia and ciliary membranes. *J. Cell Biol.* 84:717–738.

Allen, R. D. 1974. Food vacuole membrane growth with microtubule-associated membrane transport in *Paramecium*. *J. Cell Biol.* 63:904–922.

Allen, R. D. 1975. Evidence for firm linkages between microtubules and membrane-bounded vesicles. *J. Cell Biol.* 64:497–503.

Allen, R. D. 1984. *Paramecium* phagosome membrane: from oral region to cytoproct and back again. *J. Protozool.* 31:1–6.

Allen, R. D., and A. K. Fok. 1983*a*. Phagosome fusion vesicles of *Paramecium*. II. Freeze-fracture evidence for membrane replacement. *Eur. J. Cell Biol.* 29:159–165.

Allen, R. D., and A. K. Fok. 1983*b*. Nonlysosomal vesicles (acidosomes) are involved in phagosome acidification in *Paramecium*. *J. Cell Biol.* 97:566–570.

Allen, R. D., J. Metuzals, I. Tasaki, S. T. Brady, and S. P. Gilbert. 1982. Fast axonal transport in squid giant axon. *Science (Wash. DC).* 218:1127–1129.

Allen, R. D., D. G. Weiss, J. H. Hayden, D. T. Brown, H. Fujiwake, and M. Simpson. 1985. Gliding movement of and bidirectional transport along single native microtubules from squid axoplasm: evidence for an active role of microtubules in cytoplasmic transport. *J. Cell Biol.* 100:1736–1752.

Allen, R. D., C. C. Schroeder, and A. K. Fok. 1989. An investigation of mitochondrial inner membranes by rapid-freeze deep-etch techniques. *J. Cell Biol.* 108:2233–2240.

Bell, C. W., C. L. Fraser, W. S. Sale, W.-J. Y. Tang, and I. R. Gibbons. 1982. Preparation and properties of dynein ATPase. *Methods Enzymol.* 85:450–474.

Brady, S. T., R. J. Lasek, and R. D. Allen. 1982. Fast axonal transport in extruded axoplasm from squid giant axon. *Science (Wash. DC).* 218:1129–1131.

Brady, S. T., R. J. Lasek, and R. D. Allen. 1985. Video microscopy of fast axonal transport in extruded axoplasm: a new model for study of molecular mechanisms. *Cell Motil.* 5:81–101.

Collins, C. A., and R. B. Vallee. 1989. Preparation of microtubules from rat liver and testis: cytoplasmic dynein is a major microtubule associated protein. *Cell Motil. Cytoskeleton.* 14:491–500.

Dabora, S. L., and M. P. Sheetz. 1988. Cultured cell extracts support organelle movement on microtubules *in vitro*. *Cell Motil. Cytoskeleton.* 10:482–495.

Euteneuer, U., M. P. Koonce, K. K. Pfister, and M. Schliwa. 1988. An ATPase with properties expected for the organelle motor of the giant amoeba, *Reticulomyxa*. *Nature (Lond.).* 332:176–178.

Fok, A. K., and R. D. Allen. 1979. Axenic *Paramecium caudatum*. I. Mass culture and structure. *J. Protozool.* 26:463–470.

Fok, A. K., and R. D. Allen. 1988. The lysosome system. *In* Paramecium. H.-D. Gortz, editor. Springer-Verlag, Berlin. 301–324.

Fok, A. K., and R. D. Allen. 1990. The phagosome-lysosome membrane system and its regulation in *Paramecium*. *Int. Rev. Cytol.* 123:61–94.

Fok, A. K., M. S. Ueno, and R. D. Allen. 1986. Differentiation of *Paramecium* phagosome membrane and stages using monoclonal antibodies. *Eur. J. Cell Biol.* 40:1–8.

Foltz, K. R., and D. J. Asai. 1988. Ionic strength-dependent isoforms of sea urchin egg dynein. *J. Biol. Chem.* 263:2878–2883.

Gibbons, I. R. 1989. Microtubule-based motility: an overview of a fast moving field. *In* Cell Movement, Volume I. The Dynein ATPases. F. D. Warner, P. Satir, and I. R. Gibbons, editors. Alan R. Liss Inc., New York. 3–22.

Gibbons, I. R., A. Lee-Eiford, G. Mocz, C. A. Phillipson, W.-J. Y. Tang, and B. H. Gibbons. 1987. Photosensitized cleavage of dynein heavy chains. *J. Biol. Chem.* 262:2780–2786.

Heidemann, S. R., and J. R. McIntosh. 1980. Visualization of the structural polarity of microtubules. *Nature (Lond.).* 286:517–519.

Hirokawa, N., R. Sato-Yoshitake, T. Yoshida, and T. Kawashima. 1990. Brain dynein (MAP 1c) localizes on both anterogradely and retrogradely transported membranous organelles in vivo. *J. Cell Biol.* 111:1027–1037.

Koonce, M. P., and J. R. McIntosh. 1990. Identification and immunolocalization of cytoplasmic dynein in *Dictyostelium*. *Cell Motil. Cytoskeleton.* 15:51–62.

Koonce, M. P., U. Euteneuer, K. L. McDonald, D. Menzel, and M. Schliwa. 1986. Cytoskeletal architecture and motility in a giant freshwater amoeba, *Reticulomyxa*. *Cell Motil. Cytoskeleton.* 6:521–533.

Laemmli, U. K. 1970. Cleavage of structural proteins during the assembly of the head of bacteriophage T4. *Nature (Lond.).* 227:680–685.

Lanzetta, P. A., L. J. Alvarez, P. S. Reinach, and O. A. Candia. 1979. An improved assay for nanomole amounts of inorganic phosphate. *Anal. Biochem.* 100:95–97.

Marchese-Ragona, S. P., J. S. Wall, and K. A. Johnson. 1988. Structure and mass analysis of 14S dynein obtained from *Tetrahymena* cilia. *J. Cell Biol.* 106:127–132.

Martin, R. G., and B. N. Ames. 1961. A method for determining the sedimentation behavior of enzymes: application to protein mixtures. *J. Biol. Chem.* 236:1372–1379.

Merril, C. R., D. Goldman, S. A. Sedman, and M. H. Ebert. 1981. Ultrasensitive stain for proteins in polyacrylamide gels show regional variation in cerebrospinal fluid proteins. *Science (Wash. DC).* 211:1437–1438.

Neely, M. D., and K. Boekelheide. 1988. Sertoli cell processes have axoplasmic features: an ordered microtubule distribution and an abundant high molecular weight microtubule-associated protein (cytoplasmic dynein). *J. Cell Biol.* 107:1767–1776.

Neely, M. D., H. P. Erickson, and K. Boekelheide. 1990. HMW-2, the Sertoli cell cytoplasmic dynein from rat testis, is a dimer composed of nearly identical subunits. *J. Biol. Chem.* 265:8691–8698.

Paschal, B. M., and R. B. Vallee. 1987. Retrograde transport by the microtubule-associated protein MAP 1C. *Nature (Lond.).* 330:181–183.

Paschal, B. M., H. S. Shpetner, and R. B. Vallee. 1987. MAP 1C is a microtubule-activated ATPase which translocates microtubules in vitro and has dynein-like properties. *J. Cell Biol.* 105:1273–1282.

Paschal, B. M., R. A. Obar, and R. B. Vallee. 1989. Interaction of brain cytoplasmic dynein and MAP 2 with a common sequence at the C terminus of tubulin. *Nature (Lond.).* 342:569–572.

Porter, M. E., P. M. Grissom, J. M. Scholey, E. D. Salmon, and J. R. McIntosh. 1988. Dynein isoforms in sea urchin eggs. *J. Biol. Chem.* 263:6759–6771.

Pratt, M. M. 1986. Homology of egg and flagellar dynein. *J. Biol. Chem.* 261:956–964.

Rebhun, L. I. 1972. Polarized intracellular particle transport: saltatory movements and cytoplasmic streaming. *Int. Rev. Cytol.* 32:93–137.

Schnapp, B. J., and T. S. Reese. 1989. Dynein is the motor for retrograde axonal transport of organelles. *Proc. Natl. Acad. Sci. (USA).* 86:1548–1552.

Schroer, T. A., B. J. Schnapp, T. S. Reese, and M. P. Sheetz. 1988. The role of kinesin and other soluble factors in organelle movement along microtubules. *J. Cell Biol.* 107:1785–1792.

Schroer, T. A., E. R. Steuer, and M. P. Sheetz. 1989. Cytoplasmic dynein is a minus end-directed motor for membranous organelles. *Cell.* 56:937–946.

Shimizu, T. 1987. The substrate specificity of dynein from *Tetrahymena* cilia. *J. Biochem. (Tokyo).* 102:1159–1165.

Shpetner, H. S., B. M. Paschal, and R. B. Vallee. 1988. Characterization of the microtubule-activated ATPase of brain cytoplasmic dynein (MAP 1C). *J. Cell Biol.* 107:1001–1009.

Travis, S. M., and D. L. Nelson. 1988. Purification and properties of dyneins from *Paramecium* cilia. *Biochim. Biophys. Acta.* 966:73–83.

Vale, R. D., and Y. Y. Toyoshima. 1989. Microtubule translocation properties of intact and proteolytically digested dyneins from *Tetrahymena* cilia. *J. Cell Biol.* 108:2327–2334.

Vale, R. D., T. S. Reese, and M. P. Sheetz. 1985*a*. Identification of a novel

force-generating protein, kinesin, involved in microtubule-based motility. *Cell.* 42:39–50.

Vale, R. D., B. J. Schnapp, T. Mitchison, E. Steuer, T. S. Reese, and M. P. Sheetz. 1985*b*. Different axoplasmic proteins generate movement in opposite directions along microtubules in vitro. *Cell.* 43:623–632.

Vale, R. D., B. J. Schnapp, T. S. Reese, and M. P. Sheetz. 1985*c*. Movement of organelles along filaments dissociated from the axoplasm of the squid giant axon. *Cell.* 40:449–454.

Vallee, R. B. 1982. A taxol-dependent procedure for the isolation of microtubules and microtubule-associated proteins (MAPs). *J. Cell Biol.* 92:435–442.

Vallee, R. B. 1986. Purification of brain microtubules and microtubule-associated protein 1 using taxol. *Methods Enzymol.* 134:104–115.

Vallee, R. B., J. S. Wall, B. M. Paschal, and H. S. Shpetner. 1988. Microtubule-associated protein 1C from brain is a two-headed cytosolic dynein. *Nature (Lond.).* 332:561–563.